Journal of Marine Research, 76, 47–62, 2018

High-Frequency Variability in the North Icelandic Jet

by B. E. Harden[1,2] and R. S. Pickart[1]

ABSTRACT

We describe the high-frequency variability in the North Icelandic Jet (NIJ) on the Iceland Slope using data from the densely instrumented Kögur mooring array deployed upstream of the Denmark Strait sill from September 2011 to July 2012. Significant sub-8-day variability is ubiquitous in all moorings from the Iceland slope with a dominant period of 3.6 days. We attribute this variability to topographic Rossby waves on the Iceland slope with a wavelength of 62 ± 3 km and a phase velocity of 17.3 ± 0.8 km/day^{-1} directed downslope ($-9°$ relative to true-north). We test the theoretical dispersion relation for these waves against our observations and find good agreement between the predicted and measured direction of phase propagation. We additionally calculate a theoretical group velocity of 36 km day^{-1} directed almost directly up-slope (106° relative to true-north) that agrees well with the propagation speed and direction of observed energy pulses. We use an inverse wave tracing model to show that this wave energy is generated locally, offshore of the array, and does not emanate from the upstream or downstream directions along the Iceland slope. It is hypothesized that either the meandering Separated East Greenland Current located seaward of the NIJ or intermittent aspiration of dense water into the Denmark Strait Overflow are the drivers of the topographic waves.

Keywords: Topographic waves, Denmark Strait, AMOC, North Icelandic Jet

1. Introduction

The Denmark Strait Overflow is the major pathway of dense water out of the Nordic Seas. It transports 3.2 Sv, or approximately 50%, of the total outflow (Dickson and Brown 1994; Jochumsen et al. 2017), and hence plays a crucial role in the Atlantic meridional overturning circulation (AMOC). Although the existence of this overflow has been known for many decades, our understanding of the processes that govern it and the underlying dynamics remains incomplete. One important aspect that requires further study is determining the upstream sources of the dense water and how it approaches the sill. If we are to determine how a changing climate might impact the AMOC, we need to understand better the connection between the water mass transformation process and the flux of newly ventilated water to Denmark Strait.

1. Woods Hole Oceanographic Institution, Woods Hole, MA 02543, USA.
2. Corresponding author ***e-mail: bharden@sea.edu***

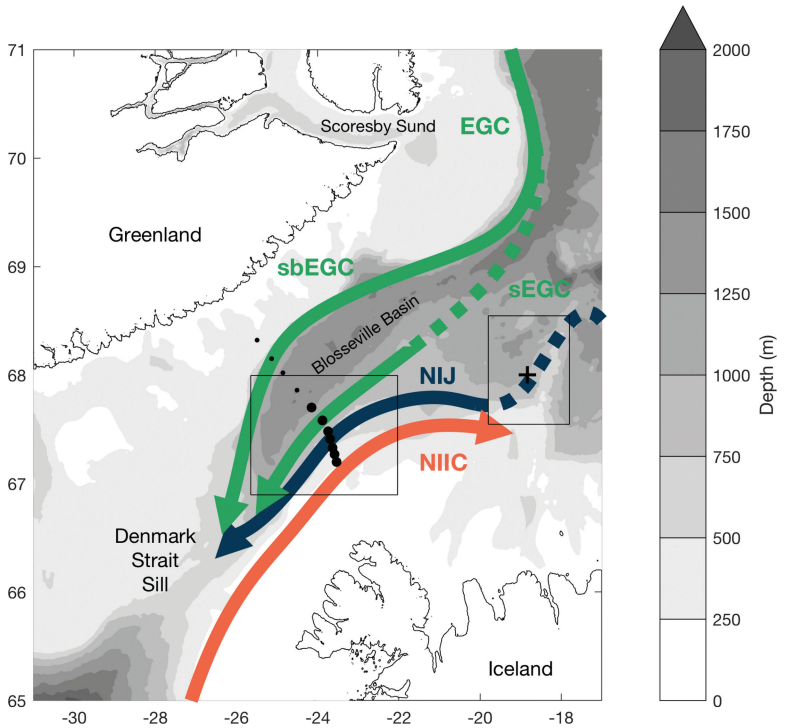

Figure 1. Map of the study region showing the overflow pathways approaching the Denmark Strait Sill: the North Icelandic Jet (NIJ) and the two East Greenland Current (EGC) pathways, one along the shelfbreak (sbEGC) and the other in a separated branch on the Iceland Slope (sEGC). Dashed portions show parts of pathways that still need further clarification. Also shown is the northward flowing surface-intensified current, the North Icelandic Irminger Current (NIIC). Black dots show the locations of the moorings in the Kögur array with larger dots indicating the subset of seven moorings used in this study. The upstream cross is the mooring to the west of the Kolbeinsey ridge referred to in the text. The bathymetry is from IBCAO v3. The inset boxes are the domains shown in Figures 4 (left) and 7 (right).

Most of the Denmark Strait Overflow water (approximately 70%) comes from the East Greenland Current by way of the Nordic Seas boundary current system (Våge et al. 2013; Harden et al. 2016; see Fig. 1). Specifically, warm Atlantic inflow across the Greenland–Scotland Ridge is progressively cooled as it flows northward towards Fram Strait, much of it recirculating in the strait and subducting to mid-depth (Mauritzen 1996). This is joined by Atlantic water exiting the strait that has circumnavigated the Arctic, and together the transformed Atlantic water flows southward in the East Greenland Current. As the current rounds Scoresby Sund, it splits into two branches (Fig. 1). One continues towards the sill as a shelfbreak jet (Håvik et al. 2017). The other carries approximately 60% of the East Greenland Current water out into the central strait via eddies and/or gyre-like deflections

of the shelfbreak jet (Våge et al. 2013; Harden et al. 2016). This interior pathway, known as the separated East Greenland current, then flows into the strait along the outer Iceland slope.

The remaining 30% of Denmark Strait Overflow water is supplied by the North Icelandic Jet (NIJ), a more recently-discovered branch of the upstream circulation (Jonsson and Valdimarsson 2004; Våge et al. 2011). This mid-depth intensified jet advects waters distinct from those found in the East Greenland Current (colder and fresher) suggestive of a source in the central Iceland or Greenland seas (Våge et al. 2011, 2015; Harden et al. 2016). The NIJ contains the densest water that feeds the overflow; its waters are found in the deepest part of the sill (Mastropole et al. 2017) and subsequently sink to the deepest depths in the core of the overflow.

The leading hypothesis for the formation of the NIJ, supported by both models and observations, is that it represents the lower limb of a local overturning cell in the Iceland Sea (Våge et al. 2011; Behrens et al. 2017). The upper limb of the cell is the North Icelandic Irminger Current (NIIC), which sheds warm water into the Iceland Sea that is cooled by air–sea heat loss. The transformed water then returns southward towards the boundary where it sinks and forms the NIJ. However, many questions remain unanswered about this proposed system. For instance, the winter mixed-layers in the Iceland Sea don't seem to be dense enough to account for the deepest water in the NIJ (Våge et al. 2015), whereas those in the Greenland Sea do (Strass et al. 1993; Rudels et al. 2002).

Regardless of the source of the NIJ, it clearly constitutes a vital component of the circulation upstream of the sill. Harden et al. (2016) investigated the jet's mean and seasonal contribution to the overflow, demonstrating that there is time-dependent partitioning of transport between the NIJ and the other two overflow branches on weekly to monthly timescales, likely driven by the wind. Pickart et al. (2017) noted that the NIJ seems to be coupled to the northward-flowing NIIC and that, on occasion, it consists of multiple branches. Using historical hydrographic data, Pickart et al. (2017) also revealed a clear link between the interannually varying properties of the NIJ and those of the densest water at the Denmark Strait sill, leaving little doubt that the NIJ is a major source of the overflow plume.

It has long been known that the Denmark Strait Overflow varies on short (order days) timescales (Smith 1976; Bruce 1995; Käse, Girton, and Sanford 2003). Some of this variability is associated with the passage of lenses of cold, dense overflow water referred to as boluses (Cooper 1955). Recently, von Appen et al. (2017) identified a second type of mesoscale feature in the strait that was termed a pulse. In contrast to boluses, pulses correspond to a thinning of the overflow layer associated with a large increase in equatorward velocity. Both of these features have been identified in a high-resolution regional model as well (Almansi et al. 2017). von Appen et al. (2017) showed that, taking into account both boluses and pulses, a mesoscale feature passes through Denmark Strait on average every 2 days. Presently, however, it is unknown if these disturbances originate from upstream or if they are associated with local dynamics near the sill.

The goal of the present study is to shed light on some of the above processes by describing the high-frequency variability of the NIJ north of the Denmark Strait. We use timeseries data from a year-long mooring array that was maintained roughly 200 km upstream of the sill (Fig. 1). This is the same data set used by Harden et al. (2016) to investigate the mean and seasonal attributes of the NIJ. Although Harden et al. (2016) mentioned that the NIJ shows high-frequency variability, they did not elaborate on this. We begin with a brief description of the data, followed by a characterization of the high-frequency signal. We discuss how this signal is consistent with the existence of topographic Rossby waves on the Iceland slope and then investigate the source region of the energy in these waves through inverse wave tracing.

2. Data and Methods

The data for this study come from the densely instrumented Kögur mooring array spanning the Denmark Strait approximately 200 km upstream of the sill. The array was deployed for 11 months from September 2011 to July 2012 and consisted of 12 moorings (named KGA 1–12) equipped with instrumentation to measure both the hydrography and velocity of the water column from 50 m to the bottom. Harden et al. (2016) present a detailed description of the mooring data, including the instrumentation, processing steps, and sensor accuracies. The array captured the majority of the overflow water ($\sigma_\theta > 27.8$ kg m^{-3}) passing through the northern part of the strait towards the sill.

Here we use primarily the gridded product described in Harden et al. (2016), which has a lateral resolution of 8 km and vertical resolution of 50 m. Because of our focus on the Iceland slope, we consider a subset of these data up to and including the location of mooring KGA 7, approximately 70 km offshore of the Iceland shelfbreak. The mean velocity sections demonstrate that this portion of the array captures both the NIJ and the majority of the Separated EGC (Fig. 2). For parts of the analysis we also use the data on a mooring-by-mooring basis. All of the velocities have been subjected to a 36-hour low-pass butterworth filter to remove the predominant M2 tidal constituent.

Additional data come from a mooring located approximately 200 km upstream of the Kögur Array on the west side of the Kolbeinsey Ridge (68°00′N, 18°50′W; see Fig. 1) This was deployed on the 1,000 m isobath from September 2007 to mid-October 2008 and consisted of a McLane Moored Profiler and acoustic current meter providing profiles between 100 m and the bottom twice daily. As with the Kögur data, we low-passed the velocity timeseries using a 36-hr filter to remove the M2 tidal component of the flow. These data are described in greater detail by Jónsson and Valdimarsson (2012).

The inverse wave tracing of topographic Rossby waves (TRWs) was done using the model described by Meinen et al. (1993) and implemented by Pickart (1995) for investigating TRWs in the Deep Western Boundary Current off of Cape Hatteras, North Carolina. The method uses the TRW dispersion relation (Eqs. 2) to calculate the group velocity (Eqs. 3 and 4) and then backtracks the evolution of the wave with a time step of 30 minutes. The

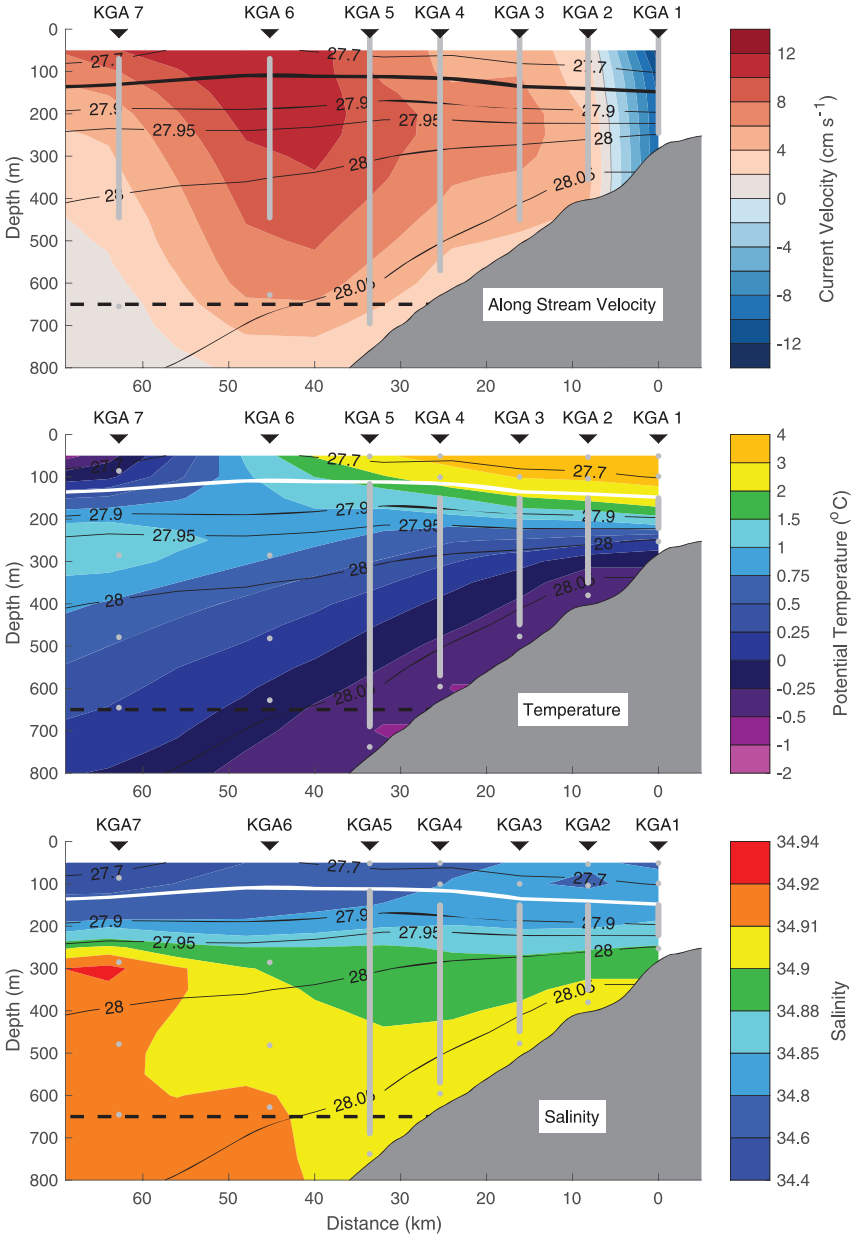

Figure 2. Mean vertical section of the along-stream (cross-transect) velocity (top) and median sections of potential temperature (middle) and salinity (bottom) for the 11-month period of the Kögur array. Overlaid in black contours on each panel is the mean density with the 27.8 kg m^{-3} isopycnal (the upper boundary of Denmark Strait Overflow Water) highlighted. The viewer is looking to the northeast with Iceland on the right. Positive velocities are equatorward. The horizontal black dashed line indicates the depth of the Denmark Strait sill. The moorings (black triangles) are labeled, and the average instrument locations are shown by the grey points. The bathymetry is from a shipboard echosounder.

wave parameters and dispersion relation are recalculated at each step for the local bottom depth, bottom slope, and water column stratification. A new group velocity is then found and used to further trace the wave. In addition, given that the calculated group velocities of the waves are comparable with the magnitude of the mean flow, we also correct the propagation paths for the mean velocities (calculated as a function of the underlying bathymetry).

Most of the required input parameters for the inverse wave-tracing model come directly from the moored data and are the same as those used for the theoretical TRW dispersion relation calculations (see Section 3a). For the bathymetry we used the International Bathymetric Chart of the Arctic Ocean 30-arcsec gridded product (Jakobsson et al. 2012). To remove seamounts and other sharp topographic features we smoothed the bathymetry using a filter of 60 km (comparable with our measured TRW wavelength). In contrast to Pickart (1995), who subsequently fit splines to the data to be able to find the bottom depth and gradients at any location, we deemed our resolution to be high enough (and our smoothing window great enough) to simply use linear interpolation. The total integration period for the wave tracing was 48 hours.

3. Results

As discussed in Harden et al. (2016), the vertical sections of velocity and hydrography at the Kögur site show the signatures of both the NIJ and the Separated EGC. However, in the mean the two features are merged to some degree and hence do not appear as distinct cores (Fig. 2). Previous synoptic sections (Våge et al. 2011) and the water mass properties recorded in this array allow us to visualize this system as two currents though. The NIJ is on the upper Iceland slope and is characterized by a mid-depth intensified flow carrying the coldest, densest overflow water banked up on the slope. The Separated EGC is farther offshore; its key features are a surface intensification and the transport of warmer, saltier overflow water at approximately 300 m. In the mean section the transition between the currents occurs at approximately 35 km offshore (Fig. 2), although synoptically the two currents are often completely separate (Harden et al. 2016). Inshore of the NIJ, on the Iceland shelf, is the poleward flowing North Icelandic Irminger Current (NIIC; see also Fig. 1).

The two overflow currents vary strongly on short timescales. This is evident by considering the timeseries of depth-averaged alongstream and cross-stream velocities, which is shown for the mooring in the core of the NIJ in Figure 3. To quantify this high-frequency variability we computed the wavelet spectrum of the depth-averaged velocity using Morlet wavelets (Lilly 2017). This is shown for the NIJ mooring in Figure 3. One sees that the signal is concentrated at sub-8-day periods with a maximum average energy at 3.6 days. As such, we high-passed the velocity timeseries using an 8-day butterworth filter. Different period filters were implemented, ranging in length from 4 days to 30 days, but the 8-day filter was most effective in isolating the peak high-frequency energy.

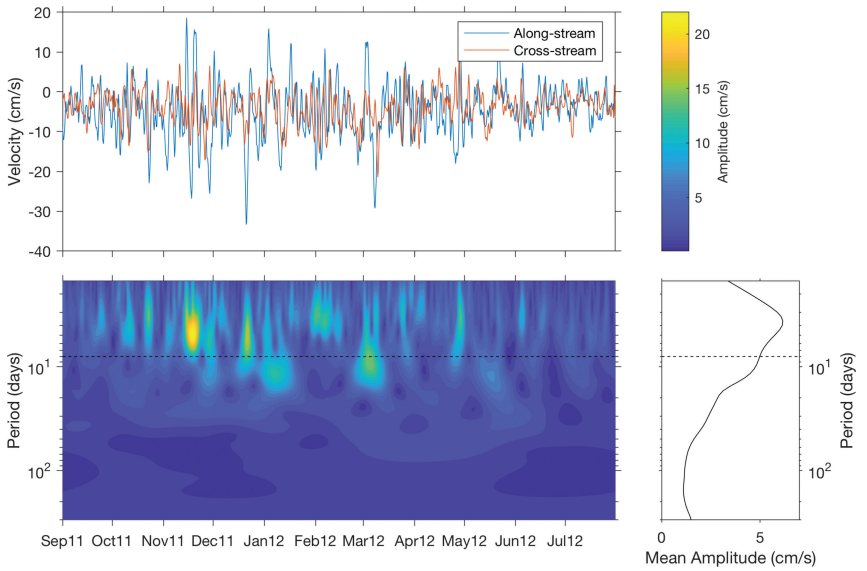

Figure 3. Top: Depth-averaged along-stream (blue) and cross-stream (red) components of velocity for the grid point closest to mooring KGA 3. Bottom left: Wavelet spectrum of the depth-averaged velocity. This was done using the jLab toolbox (Lilly 2017) with standard Morlet wavelets with $\gamma = 3$ and $\beta = 2$. The color scale for this plot is at the top right. Bottom right: Mean wavelet amplitude for the length of the deployment. The dashed line in the bottom panels indicates the 8-day cut-off period for the high-pass filter used in the study.

The high-passed current ellipses for each mooring are useful for characterizing different regimes across the array (Fig. 4). In the NIIC (KGA 1), the current ellipse is elongated in the direction of the mean flow indicative of a current pulsing along its axis. By contrast, within the Separated EGC (KGA 6 and 7), the elongation of the current ellipses is perpendicular to the mean flow, demonstrating that this current meanders. However, in the NIJ (KGA 2–4), the major axes of the current ellipses are aligned at an oblique angle to both the mean flow and the underlying bathymetry. This is characteristic of topographic Rossby waves (TRWs) (Pickart and Watts 1990). KGA 5 seems to be in a transition region between conditions in the NIJ and those in the Separated EGC.

Another perspective of the high-frequency variability present across the array is obtained by computing Hovmöller plots. We did this for the depth-mean along-stream velocity, which is shown in Figure 5a. On the Iceland slope (inshore of approximately 50 km), the sub-8-day period signal dominates throughout the record. Farther offshore, however, in the vicinity of the Separated EGC, there is also a lower frequency signal on timescales of weeks to months. These more slowly varying fluctuations were described by Harden et al. (2016) and attributed in part to the time-varying upstream bifurcation of the EGC. We now investigate the nature of the sub-8-day variability.

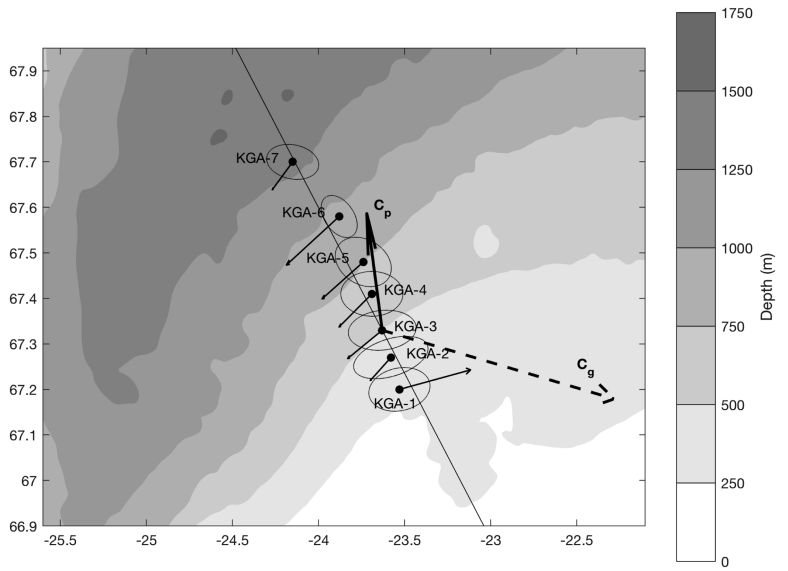

Figure 4. Aspects of the flow measured by the Kögur moorings (black circles). The thin vectors indicate the mean velocity averaged from 100 m to the depth of the ADCP at each mooring (see gray lines in Fig. 2). Also shown are the 8-day high-passed current ellipses for the same depth range. The thick black arrow (C_p) denotes the direction of TRW phase propagation averaged over KGA 2–4 (plotted at KGA 3). The dashed black arrow shows the direction of TRW group velocity (C_g). All vectors and current ellipses are drawn to the same scale as indicated. The long black line is the mean downslope direction averaged between KGA 2–4. The bathymetry is from IBCAO v3.

a. Topographic Rossby waves

We resolved the sub-8-day depth-averaged flow in the gridded product along the major axis of the current ellipses at each offshore location. Particularly in the NIJ, the variability along these axes have a sinusoidal form and are lagged between moorings such that the pulses of current progress offshore in time (Fig. 5b). This implies a downslope phase propagation of this variability.

We argue that this is the signature of TRWs. These waves are supported by topographic β and result in transverse fluctuations that are often at an oblique angle to the mean flow (recall the orientation of the 8-day variance ellipses in the vicinity of the NIJ; Fig. 4). TRWs are found in many slope regions of the world's oceans (Garrett 1979; Louis, Petrie, and Smith 1982; Pickart and Watts 1990). Key features of TRWs include wave vectors (and hence phase velocities) that are perpendicular to the velocity variability, a group velocity that is at an oblique angle to the phase velocity, and a tendency to be bottom-trapped in regions of significant stratification.

Given that the phase propagation is perpendicular to the velocity variability, we deduce that the wave phase is progressing downslope at −9°T (where °T refers to degrees relative to

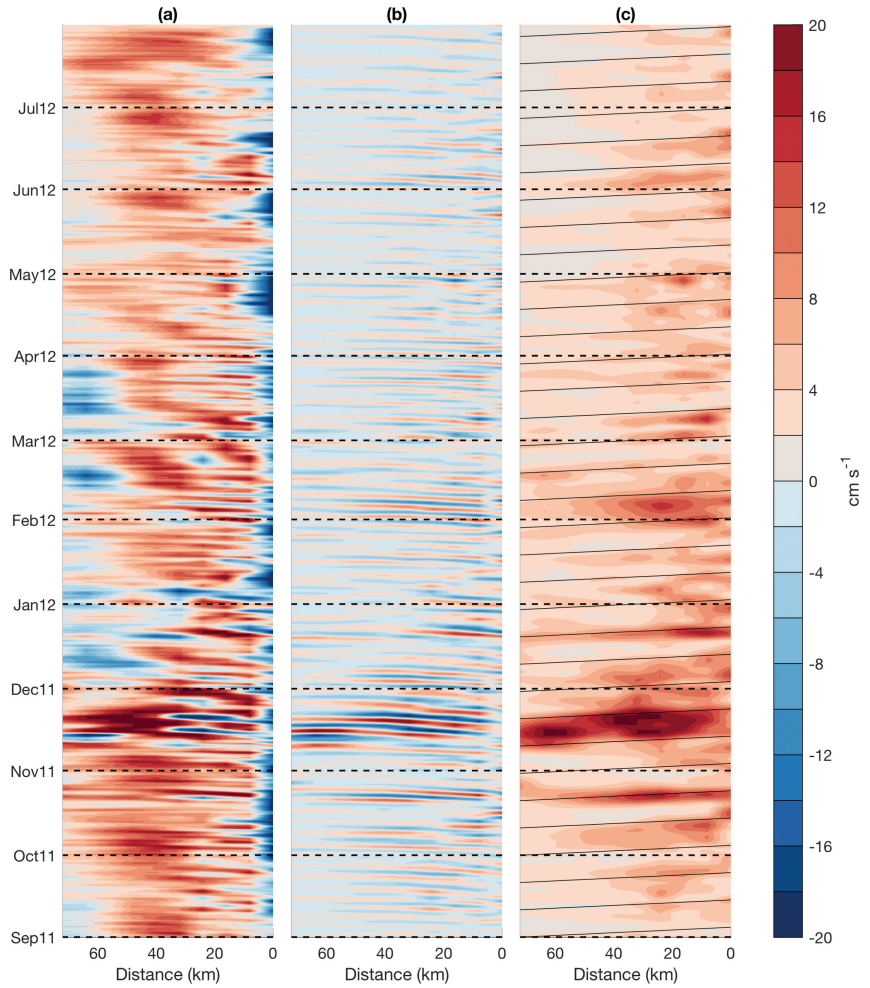

Figure 5. Hovmöller plots from the gridded mooring data of a) the depth-mean along-stream velocity (below 100 m, same for all plots); b) the 8-day high-passed, depth-mean component of velocity in the direction of the major axis of the local current ellipse; and c) the wavelet amplitude at a 4-day period for the depth-mean velocity. Iceland is to the right of each panel, as in Figure 2. The sloped, black guidelines in panel c are angled at the theoretical group velocity for the measured topographic Rossby waves (see text for details).

true north). This value is the average direction over KGA 2–4, where we see the most direct evidence for TRWs (see Fig. 4). Following Pickart and Watts (1990), we then calculated the phase speed over the range of moorings KGA 2–4 using

$$c_p = \frac{1}{T}\,\frac{360}{\overline{\phi}}\,\frac{\overline{\Delta S}}{cos(\Delta)} \tag{1}$$

where T is the wave period (= 3.6 days), $\overline{\phi}$ is the average phase offset (= 48 ± 3 °), $\overline{\Delta S}$ is the average instrument spacing (= 8.1 ± 0.2 km), and Δ is the angle between the mooring array and the direction of wave propagation (= 8 ± 4 °). This equation is essentially a geometric calculation that adjusts the wave propagation speed observed between moorings to being along the wave vector instead.

The resulting phase speed is 17.3 ± 0.8 km day^{-1} corresponding to a wavelength of 62 ± 3 km. The error estimates arise in equal contributions from uncertainties in $\overline{\phi}$, $\overline{\Delta S}$, and Δ.

As a consistency check that the observed fluctuations are in fact TRWs, we can employ the TRW dispersion relation for waves in a uniformly stratified ocean over a linearly sloping bottom, with a rigid lid and neglecting planetary β. This result is derived in non-dimensional units in Pedlosky (1979) and can be written in dimensional units (following Pickart 1995) as follows:

$$T = \frac{2\pi\, tanh\left(\frac{2\pi ND}{\lambda f}\right)}{N\Gamma sin(\theta)} \tag{2}$$

where T is the period of the wave (3.6 days), N is the average water column Brunt Väisälä frequency (= 3.3×10^{-5}, averaged using the gridded data below 100 m), D is the depth (= 500 m), λ is the scalar wavelength (62 km), f is the Coriolis parameter (= 1.35×10^{-4}), Γ is the bottom slope (= 0.016, from IBCAO v3), and θ is the phase velocity direction relative to downslope.

Using Equation 2 we obtain a predicted value of θ = 29 ° using our knowledge of the other variables. This predicted value compares well with the measured value of 24 ° (from the average downslope angle between moorings KGA 2–4). There is of course uncertainty in the measured downslope angle depending on the region selected for the averaging. For example, if we expand the calculation of the downslope direction to encompass KGA 1–5, the measured θ becomes 33 °, which still agrees well with the predicted value. In addition, the bottom-trapping scale (= $f/N\,k$) is much greater than 1,000 m, in agreement with the observed velocities that are largely barotropic.

All of this supports our assertion that the dominant high-frequency variability in the NIJ is due to TRWs. The obvious question is, where and how are these waves being generated? Using the dispersion relation we can calculate the group velocity (C_g), which can be written as follows:

$$C_{gx} = \frac{\partial\sigma}{\partial k} = N\Gamma\left(\frac{\lambda cos^2\theta}{2\pi\, tanh\left(\frac{2\pi ND}{\lambda f}\right)} - \frac{NDsin^2\theta}{fsinh^2\left(\frac{2\pi ND}{\lambda f}\right)}\right), \tag{3}$$

$$C_{gy} = \frac{\partial\sigma}{\partial l} = -\frac{1}{2}N\Gamma sin(2\theta)\left(\frac{\lambda}{2\pi\, tanh\left(\frac{2\pi ND}{\lambda f}\right)} + \frac{ND}{fsinh\left(\frac{2\pi ND}{\lambda f}\right)}\right) \tag{4}$$

where the x and y subscripts are for the group velocities in the along-slope (positive poleward) and cross-slope (positive down-slope) directions, respectively, k and l are the wave

vectors in the x and y directions, and σ is the angular frequency of the wave ($2\pi/T$). The rest of the parameters are defined above for Equation 2.

For the observed parameters, we find the magnitude of the group velocity to be 36 km day^{-1} directed up-slope at the array site (106°T; see Fig. 4). This implies that the energy source lies offshore. We can corroborate this onshore propagation of energy observationally by considering the wavelet amplitude for the 4-day signal at each mooring site. The Hovmöller plot in Figure 5c shows clear occurrences of onshore energy propagation that are in line with the predicted group velocity, which contrasts with the offshore phase propagation in Figure 5b. Particularly good examples of this onshore energy propagation occur in mid-November, late December, early February, and early June.

b. Wave tracing and TRW formation mechanisms

In order to shed light on the source of the TRWs, we implemented the inverse wave-tracing model described in Section 2. In particular, we calculated the wave paths backwards in time from moorings KGA 2–4. For each mooring, the model was initialized with the local wavenumber (assuming constant phase velocity and wave period across the array). As stated in Section 2, we also incorporate the mean flow into our wave tracing, which impacts the inverse traces to some extent (bends them in the upstream direction).

The calculated paths indicate that the waves originate offshore of the moorings in the vicinity of the deep Blosseville Basin (Fig. 6). The traces from KGA2–4 do not show any significant deflection in the upstream or downstream directions. Although they diverge somewhat as they head downslope, it is clear that the TRW energy does not emanate from either the Denmark Strait or from upstream in the Iceland Sea but, instead, originates locally.

TRWs are a ubiquitous feature in the middle Atlantic Bight between Cape Hatteras, North Carolina and the Grand Banks of Newfoundland (Louis, Petrie, and Smith 1982; Johns and Watts 1986; Pickart and Watts 1990). The source of the waves appears to be the Gulf Stream. Both Hogg (1981) and Schultz (1987) argued that TRWs observed along the US continental slope emanated from large amplitude Gulf Stream meanders offshore. Louis, Petrie, and Smith (1982) made the case that bursts of TRWs measured south of Nova Scotia resulted from Gulf Stream eddy formation. Pickart (1995) demonstrated that the TRWs observed near Cape Hatteras were forced by meanders of the Gulf Stream as it flowed over a bend in topography farther to the east.

In light of these studies, it is natural to suspect that the TRWs measured at the Kögur array site are generated by the Separated EGC. This current is energetic, and, as noted above, is subject to meandering (akin to the Gulf Stream). The wave tracing indicates that the TRW energy emanates from the Blosseville Basin where the Separated EGC resides. Additionally, there is evidence in Figure 5c that times of strong TRW activity on the upper slope are often preceded by increases in meander energy in the Separated EGC. Recall that the velocities in Figure 5b and c are rotated along the major axis of the local variance ellipse (see Fig. 4); hence, they represent meanders offshore in the Separated EGC and

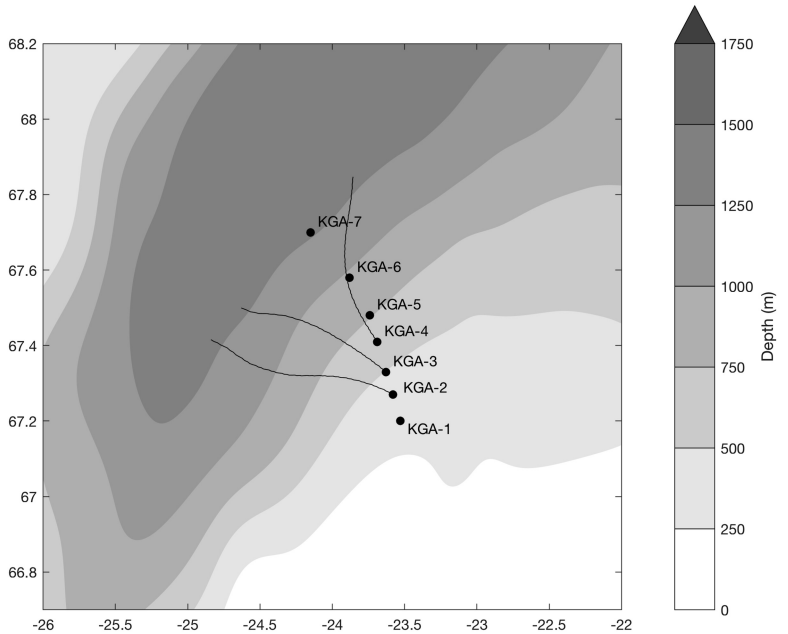

Figure 6. Ray paths of the Topographic Rossby Waves (thin lines) computed using the inverse wave tracing model for moorings KGA 2–4. Wave traces are truncated as they pass the 1,300-m isobath. The bathymetry is from IBCAO v3 smoothed over 60 km (see text for details).

TRWs onshore in the NIJ. Therefore, the signal propagation seen in Figure 5c (for example in late-October, mid-November, late-December, and early-February) can be interpreted as offshore meanders transferring energy onshore into TRWs.

Another possible trigger for the waves is the intermittent aspiration of deeper waters towards the Denmark Strait Sill. Harden et al. (2016) demonstrated that 0.6 Sv of the overflow transport approaching the sill does so from below sill depth, which necessarily must climb a topographic gradient to reach the sill. Further to that study, we also observe variability below sill depth that is aligned obliquely across the Strait (not shown) that is correlated to the TRW variability on the Iceland Slope. It is unclear at this stage what is driving this deep variability. It may be a deep-reaching expression of the meandering Seperated EGC, wave signals from the Denmark Strait Overflow downstream, or a combination of both. As we will touch on in Section 4, a complete understanding of the linkages between the variability at the sill and the full Kögur Array (all 12 moorings) will likely be necessary to definitely determine the source of deep energy in the Blosseville Basin.

Regardless of the formation mechanism, the presence of TRWs in our data raises the question of whether they are present along the entire Iceland slope or instead unique to our

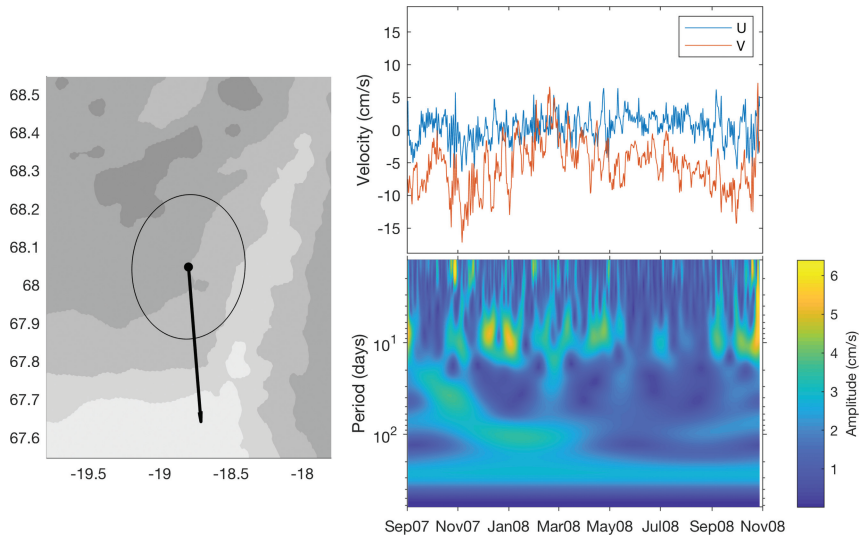

Figure 7. Flow aspects of the depth–mean current from the Kolbeinsey Ridge mooring located approximately 200 km upstream of the Kögur Array. Left: Map showing location of mooring, mean flow (vector), and current ellipse overlaid on the same topography as Figure 4. Right: As Figure 3, time series of the U (blue) and V (red) components of the velocity timeseries (top) and the wavelet spectrum of the velocity field (bottom).

sampling region. To address this we examined the velocity data from a mooring deployed approximately 200 km upstream on the Iceland slope near the Kolbeinsey Ridge from 2007–2008 (Fig. 7).

The depth–mean velocity from the upstream mooring shows predominant variability at approximately a 10-day period (Fig. 7), with much less variability in the 4-day period seen in the Kögur Array. As with KGA2–4, the major axis of the current ellipse is at an oblique angle to the mean flow, but without additional moorings at this site we are unable to assess phase propagation to determine if this variability is consistent with TRWs. However, the fact that the TRW inverse ray paths at the Kögur Array do not bend significantly upstream, together with the difference in wave frequencies between the sites, suggests that the variability at the Kolbeinsey Ridge is not dynamically linked to that at the Kögur Array. This supports our assertion that the TRWs at the Kögur Array are locally produced. Interestingly, the hydrographic data at the Kolbeinsey Ridge mooring (not shown) show clear, isolated incursions of EGC water predominantly in the wintertime. This indicates that the Separated EGC is active on the Iceland Slope this far upstream of the Denmark Strait sill, which implies that if the variability at the Kolbeinsey Ridge mooring is that of TRWs, the wave energy there could still potentially be generated by a meandering Separated EGC.

4. Summary and Discussion

We have documented the existence of energetic Topographic Rossby Waves (TRWs) within the North Icelandic Jet (NIJ) using observations from the densely-instrumented Kögur Array located approximately 200 km upstream of the Denmark Strait sill. The mean period of the waves is 3.6 days, the wavelength is 62 $\pm$ 3 km, and the phase velocity is 17.3 $\pm$ 0.8 km day^{-1} directed downslope (−9°T). Using the TRW dispersion relation, we corroborated our observed direction of phase propagation relative to the downslope direction (24°) with the theoretical value (29°). We further determined from the expression for group velocity that the wave energy is progressing up-slope (106°T) at 36 km day^{-1}, in agreement with the observational data. Based on inverse wave tracing, the energy in the TRWs seems to emanate locally from the Blossevile Basin. The most likely source is the meandering of the offshore Separated East Greenland Current (EGC), although pulses of cross-bathymetric flow due to the aspiration of deep overflow water could represent a possible source as well. Winds do not seem to play a role because they vary seasonally whereas the TRWs are ubiquitous throughout the year.

Notably, our data imply that the dominant high-frequency variability on the Iceland Slope does not originate from the Denmark Strait, nor does it propagate towards the sill. This suggests that the mesoscale features at the sill (boluses and pulses), diagnosed observationally by von Appen et al. (2017) and in a model framework by Almansi et al. (2017), are not triggered by, nor directly excite, the TRWs on the Iceland Slope. Nonetheless, the likelihood of a connection between the high-frequency variability at the two locations is still high, given the geographic proximity and the similarity in timescales, but is presumably mediated by another process. The Denmark Strait overflow is believed to be subject to hydraulic control (Whitehead 1998; Nikolopoulos et al. 2003), and, consequently, information should be transferred between the sill and the region to the north, likely as Kelvin waves. The existence of any such connection and the impact on variability at the sill and upstream in the EGC and NIJ requires further investigation and is the subject of an on-going study.

Another topic requiring further work is determining where the energy in the TRWs ends up and what impact it might have on the dynamics of the circulation inshore of the Iceland slope. Our results indicate that energy is being fluxed into the poleward-flowing North Icelandic Irminger Current (NIIC), but presently we are unable to say what impact this has on this current. Våge et al. (2011) hypothesize that, to the north of our array, an offshore flux of warm water associated with the disintegration of the NIIC is tied to the overturning loop that forms the NIJ. We know that eddies of NIIC water are found both in the Blosseville Basin (Jónsson and Valdimarsson 2012) and in the Iceland Sea (Våge et al. 2011). Future studies of the mechanisms by which the NIIC destabilizes and fluxes water offshore should take into account the source of energy directed onshore at the Kögur site and potentially farther north as well, on the Iceland Slope.

Acknowledgments. We would like to thank the crew and technicians aboard the R/V Knorr and RSS James Clark Ross for the deployment and recovery of the Kögur moorings. This work was

supported by National Science Foundation grants OCE-1433958 (BH), OCE-0959381 (BH and RP) and OCE-1558742 (RP).

REFERENCES

Almansi, M., T. W. N. Haine, R. S. Pickart, M. G. Magaldi, R. Gelderloos, and D. Mastropole. 2017. High-frequency variability in the circulation and hydrography of the Denmark Strait Overflow from a high-resolution numerical model. J. Phys. Oceanogr., *47*(12), 2999–3013. doi: 10.1175/JPO-D-17-0129.1

Behrens, E., K. Våge, B. Harden, A. Biastoch, and C. W. Böning. 2017. Composition and variability of the Denmark Strait Overflow water in a high-resolution numerical model hindcast simulation. J. Geophys. Res.: Oceans, *122*(4), 2830–2846. doi: 10.1002/2016JC012158

Bruce, J. 1995. Eddies southwest of the Denmark Strait. Deep Sea Res. Part I: Oceanogr. Res. Pap., *42*(1), 13–29. doi: 10.1016/0967-0637(94)00040-Y

Cooper, L. H. N. 1955. Deep water movements in the North Atlantic as a link between climatic changes around Iceland and biological productivity of the English Channel and Celtic Sea. J. Mar. Res., *14*, 347–362.

Dickson, R. R. and J. Brown. 1994. The production of North Atlantic Deep Water: sources, rates, and pathways. J. Geophys. Res., *99*, 12319–12341. doi: 10.1029/94JC00530

Garrett, C. 1979. Topographic Rossby waves off East Australia: identification and role in shelf circulation. J. Phys. Oceanogr., *9*, 244–253. doi: 10.1175/1520-0485(1979)009⟨0244:TRWOEA⟩2.0.CO;2

Harden, B. E., R. S. Pickart, H. Valdimarsson, K. Våge, L. de Steur, C. Richards, F. Bahr et al. 2016. Upstream sources of the Denmark Strait Overflow: observations from a high-resolution mooring array. Deep Sea Res. Part I: Oceanogr. Res. Pap., *112*, 94–112. doi: 10.1016/j.dsr.2016.02.007

Håvik, L., K. Våge, R. S. Pickart, B. Harden, W. J. von Appen, S. Jónsson, and S. Østerhus. 2017. Structure and variability of the shelfbreak East Greenland Current north of Denmark Strait. J. Phys. Oceanogr., *47*, 2631–2646. doi: 10.1175/JPO-D-17-0062.1

Hogg, N. G. 1981. Topographic waves along 70 °W on the continental rise. J. Mar. Res., *39*, 627–649.

Jakobsson, M., L. Mayer, B. Coakley, J. A. Dowdeswell, S. Forbes, B. Fridman, H. Hodnesdal et al. 2012. The International Bathymetric Chart of the Arctic Ocean (IBCAO) Version 3.0. Geophys. Res. Lett., *39*, L12609. doi: 10.1029/2012GL052219

Jochumsen, K., M. Moritz, N. Nunes, D. Quadfasel, K. M. H. Larsen, B. Hansen, H. Valdimarsson, and S. Jonsson. 2017. Revised transport estimates of the Denmark Strait overflow. J. Geophys. Res.: Oceans, *122*, 3434–3450. doi: 10.1002/2017JC012803

Johns, W. E. and D. R. Watts. 1986. Time scales and structure of topographic Rossby waves and meanders in the deep Gulf Stream. J. Mar. Res., *44*, 267–290. doi: 10.1357/002224086788405356

Jonsson, S. and H. Valdimarsson. 2004. A new path for the Denmark Strait overflow water from the Iceland Sea to Denmark Strait. Geophys. Res. Lett., *31*(3), L03305. doi: 10.1029/2003GL019214

Jónsson, S. and H. Valdimarsson. 2012. Hydrography and circulation over the southern part of the Kolbeinsey Ridge. ICES J. Mar. Sci., *69*(7), 1255–1262. doi: 10.1093/icesjms/fss101

Käse, R. H., J. B. Girton, and T. B. Sanford. 2003. Structure and variability of the Denmark Strait Overflow: model and observations. J. Geophys. Res.: Oceans, *108*, 3181. doi: 10.1029/2002JC001548

Lilly, J. M. 2017. jLab: a data analysis package for Matlab, v 1.6.3. http://www.jmlilly.net/jmlsoft.html

Louis, J. P., B. D. Petrie, and P. C. Smith. 1982. Observations of topographic rossby waves on the continental margin off Nova Scotia. J. Phys. Oceanogr., *12*, 47–55. doi: 10.1175/1520-0485(1982)012⟨0047:OOTRWO⟩2.0.CO;2

Mastropole, D., R. S. Pickart, H. Valdimarsson, K. Våge, K. Jochumsen, and J. Girton. 2017. On the hydrography of Denmark Strait. J. Geophys. Res.: Oceans, *122*, 306–321. doi: 10.1002/2016JC012007

Mauritzen, C. 1996. Production of dense overflow waters feeding the North Atlantic across the Greenland-Scotland Ridge. Part 1: evidence for a revised circulation scheme. Deep Sea Res. Part I: Oceanogr. Res. Pap., *43*, 769–806. doi: 10.1016/0967-0637(96)00037-4

Meinen, C., E. Fields, R. S. Pickart, and D. R. Watts. 1993. Ray tracing on topographic rossby waves. Technical Report 93-1, Kingston: University of Rhode Island.

Nikolopoulos, A., K. Borenäs, R. Hietala, and P. Lundberg. 2003. Hydraulic estimates of Denmark Strait overflow. J. Geophys. Res.: Oceans, *108*, 3095. doi: 10.1029/2001JC001283

Pedlosky, J. 1979. *Geophysical Fluid Dynamics*. New York: Springer US. doi: 10.1007/978-1-4684-0071-7

Pickart, R. S. 1995. Gulf Stream–generated topographic Rossby waves. J. Phys. Oceanogr., *25*, 574–586. doi: 10.1175/1520-0485(1995)025⟨0574:GSTRW⟩2.0.CO;2

Pickart, R. S. and D. R. Watts. 1990. Deep Western Boundary Current variability at Cape Hatteras. J. Mar. Res., *48*, 765–791.

Pickart, R. S., M. A. Spall, D. J. Torres, K. Våge, H. Valdimarsson, C. Nobre, G. W. K. Moore et al. 2017. The North Icelandic Jet and its relationship to the North Icelandic Irminger Current. J. Mar. Res., *75*, 605–639. doi: 10.1357/002224017822109505

Rudels, B., E. Fahrbach, J. Meincke, G. Budéus, and P. Eriksson. 2002. The East Greenland Current and its contribution to the Denmark Strait overflow. ICES J. Mar. Sci., *59*, 1133–1154. doi: 10.1006/jmsc.2002.1284

Schultz, R. J. 1987. Structure and propagation of topographic Rossby waves northeast of Cape Hatteras, North Carolina. Master's thesis, Marine Science Program, Chapel Hill. University of North Carolina.

Smith, P. C. 1976. Baroclinic instability in the Denmark Strait Overflow. J. Phys. Oceanogr., *6*, 355–371. doi: 10.1175/1520-0485(1976)006⟨0355:BIITDS⟩2.0.CO;2

Strass, V. H., E. Fahrbach, U. Schauer, and L. Sellmann. 1993. Formation of Denmark Strait overflow water by mixing in the East Greenland Current. J. Geophys. Res.: Oceans, *98*, 6907–6919. doi: 10.1029/92JC02732

Våge, K., R. S. Pickart, M. A. Spall, H. Valdimarsson, S. Jónsson, D. J. Torres, S. Østerhus, and T. Eldevik. 2011. Significant role of the North Icelandic Jet in the formation of Denmark Strait overflow water. Nat. Geosci., *4*, 723–727. doi: 10.1038/ngeo1234

Våge, K., R. S. Pickart, M. A. Spall, G. W. K. Moore, H. Valdimarsson, D. J. Torres, S. Y. Erofeeva, and J. E. Ø. Nilsen. 2013. Revised circulation scheme north of the Denmark Strait. Deep Sea Res. Part I: Oceanogr. Res. Pap., *79*, 20–39. doi: 10.1016/j.dsr.2013.05.007

Våge, K., G. W. K. Moore, S. Jónsson, and H. Valdimarsson. 2015. Water mass transformation in the Iceland Sea. Deep Sea Res. Part I: Oceanogr. Res. Pap., *101*, 98–109. doi: 10.1016/j.dsr.2015.04.001

von Appen, W. J., D. Mastropole, R. S. Pickart, H. Valdimarsson, S. Jónsson, and J. B. Girton. 2017. On the nature of the mesoscale variability in Denmark Strait. J. Phys. Oceanogr., *47*, 567–582. doi: 10.1175/JPO-D-16-0127.1

Whitehead, J. A. 1998. Topographic control of oceanic flows in deep passages and straits. Rev. Geophys., *36*, 423–440. doi: 10.1029/98RG01014

Received: *25 January 2018*; revised: *20 June 2018*.